JOURNAL OF GEOPHYSICAL RESEARCH, VOL. 111, D16110, doi:10.1029/2005JD006861, 2006

Characteristics of inertia gravity waves over the South Pacific as revealed by radiosonde observations

Miho Yamamori[1,2] and Kaoru Sato[3]

Received 8 November 2005; revised 2 March 2006; accepted 29 March 2006; published 29 August 2006.

[1] Using horizontal wind and temperature data with fine vertical resolution obtained by radiosondes, we investigate the characteristics of parameters and propagation properties of inertia gravity waves in the upper troposphere and lower stratosphere in the subtropics and extratropics over the South Pacific where very few observations have so far been done. Components extracted by a band-pass filter having cutoff vertical wavelengths of 0.5 and 5 km are analyzed as gravity waves. Gravity wave parameters such as intrinsic frequency $\hat{\omega}$, vertical and horizontal wavelengths, and phase and group velocities are estimated by hodograph analysis. The statistics on such parameters are presented for both the stratosphere and troposphere for the three latitudinal ranges 17°–24°S, 25°–33°S, and 34°–48°S. The horizontal wavelengths decrease and $\hat{\omega}$ increases with increasing latitude south. The dominant values for the Coriolis parameter f divided by $\hat{\omega}$ are ~0.5 in the lower stratosphere and ~0.3 in the troposphere, with little dependence on latitude. The dominant vertical wavelengths for upward propagating waves are longer in the troposphere than in the lower stratosphere. The most dominant direction of horizontal propagation is southward, with a little bias toward southeastward. A case study using ray tracing suggests that the major source of such southeastward waves is located in the upper troposphere. Notable northward propagation of gravity waves is also found in the subtropical lower stratosphere. The source of the gravity waves is considered to be a cutoff cyclone developing in the upper troposphere.

Citation: Yamamori, M., and K. Sato (2006), Characteristics of inertia gravity waves over the South Pacific as revealed by radiosonde observations, *J. Geophys. Res.*, *111*, D16110, doi:10.1029/2005JD006861.

1. Introduction

[2] Gravity waves play an important role in determining large-scale circulation and the thermal structure of the middle atmosphere. They are generated by various sources (for example, topography, convection and organized convection system, and spontaneous adjustment), and then propagate from the source region, and finally break or dissipate in other regions. These processes transfer horizontal momentum from the excitation level/latitude to the breaking level/latitude. Since global circulation models (GCMs) usually do not resolve the spatial scales of gravity waves except for high-resolution models [e.g., *Sato et al.*, 1999], their effects have to be parameterized to realistically simulate atmospheric circulation. The parameterization of topographically forced gravity waves was first incorporated into GCMs [e.g., *McFarlane*, 1987; *Palmer et al.*, 1986; *Iwasaki et al.*, 1989]. Subsequently, parameterization of nonstationary gravity waves was developed and introduced in GCMs [e.g., *Hines*, 1997; *Manzini et al.*, 1997; *Alexander and Dunkerton*, 1999; *Warner and McIntyre*, 2001]. Each parameterization requires specification of "source spectra", giving wave spectra at a particular altitude in terms of phase speeds, propagation direction, frequency, initial magnitudes, and vertical and horizontal wavelengths. The practical implementation into GCMs is a key issue of current concern in middle atmospheric science.

[3] As many observational studies have reported, seasonal and geographical variations in gravity wave activity are significant. Knowledge on gravity waves over landmasses has been accumulated, with the aid of ground-based radars [e.g., *Sato*, 1994], lidars [*Wilson et al.*, 1991], and radiosonde soundings on routine [*Kitamura and Hirota*, 1989; *Allen and Vincent*, 1995; *Vincent and Alexander*, 2000; *Yoshiki and Sato*, 2000; *Yoshiki et al.*, 2004] and campaign bases [*Tsuda et al.*, 1994]. However, our knowledge on gravity waves over the ocean is vastly inferior because examinations of gravity waves through observations in oceanic regions have been done through limited studies using radio soundings conducted at small islands surrounded by ocean [*Guest et al.*, 2000; *Chane-Ming et al.*, 2002] or from ships [*Plougonven et al.*, 2003]. Recently, GPS occultation technique has enabled to derive stratospheric temperature profiles regardless over land and ocean

[1]National Institute of Information and Communications Technology, Tokyo, Japan.
[2]Now at Department of Elementary Education, Tsuru University, Tsuru, Japan.
[3]Department of Earth and Planetary Science, University of Tokyo, Tokyo, Japan.

0148-0227/06/2005JD006861$09.00

[*Ware et al.*, 1996; *Rocken et al.*, 1997], and *Tsuda et al.* [2000] presented global distribution of potential energy of gravity waves using the temperature profiles.

[4] A cruise experiment, MeSSO2001 (Meridional Scan of the Stratosphere over the Ocean in 2001), was undertaken to examine the characteristics of small-scale atmospheric disturbances over the ocean with special reference to gravity waves [*Sato et al.*, 2003]. A radiosonde observation campaign was conducted to scan the stratosphere meridionally over the middle Pacific at intervals of about 1°, with enough high vertical resolution for gravity waves. As stated by *Sato et al.* [2003], it is important to observe gravity waves over the ocean not only because observation has been limited, but also because nonstationary gravity waves can more easily be observed than over landmasses. They also examined latitudinal variations in gravity wave energy and vertical wave number spectra. They found that the wave energy in tropical regions is greater than the climatology, on the basis of operational radiosonde observations over land regions, suggesting that there are significant nonstationary gravity wave sources over the ocean. The existence and importance of gravity waves propagating meridionally from the tropics toward higher latitudes were also discussed.

[5] The present paper mainly focuses on the statistics for wave parameters and the propagation characteristics of inertia gravity waves in the upper troposphere and lower stratosphere over the subtropical and extratropical South Pacific, using the MeSSO2001 radiosonde data. Observations in such oceanic regions were extremely limited compared with over the northern hemisphere and the tropics.

[6] We first describe the observations and data in section 2. The background and gravity wave fields are briefly looked at in section 3. The estimation method and characteristics of gravity wave parameters are presented in section 4. The propagation properties are discussed in section 5. Several issues, including the use of ray-tracing analysis to detect sources, are discussed in section 6. The results are summarized in section 7.

2. Description of Cruise Experiment and Data

[7] During the MeSSO2001, 84 radiosondes (Väisälä RS80-15GH) were launched from the *Hakuho-maru*, a research vessel of Ocean Research Institute (ORI) of the University of Tokyo, from 27 November to 25 December 2001. Seventy vertical profiles of temperature, horizontal winds, and relative humidity were successfully obtained over a wide latitude range from 28°N to 48°S at intervals of about 1°. When used from a mobile sounding station, the accuracy of the wind data is 0.5 m/s. Wind data with an original time interval of 0.5 s obtained by GPS observations are smoothed and recorded every 2 s corresponding to a height resolution of about 10 m. The accuracy of temperature data is 0.1 K. The data interval for temperature and relative humidity is 1.5 s or 7–8 m in the vertical direction. Because of the response time of the temperature sensor, the real vertical resolution is about 20–80 m, depending on the altitude. We interpolated the data at an interval of 50 m in the vertical direction to simplify analysis.

[8] We analyzed the horizontal wind and temperature data at 32 points from 17°S (observed on 13 December) to 48°S (observed on 23 December) along the 160°W meridian in the upper troposphere and lower stratosphere. Although the sensor launched at 24°S failed to observe horizontal winds in a height range from 5 to 14 km, all the soundings used here reached higher than 24 km. Since the ship remained stationary for 6–30 hours every 5°latitude for the oceanographic measurements, the time interval for the launches was not constant.

[9] Six-hourly European Centre for Medium-range Weather Forecasts (ECMWF) operational analysis data at 21 levels from 1000 to 1 hPa were used to examine the synoptic-scale structure of the atmosphere. The ECMWF fields of temperature and horizontal winds were also used for the ray calculations discussed in section 6.

3. Outline of Observed Structures

3.1. Background Field

[10] Figure 1 shows meridional cross sections for temperature, and zonal and meridional winds prepared with the observational and ECMWF operational data. We calculated the ECMWF data at every observation point through linear interpolation both temporally and spatially. The vertical axes for the ECMWF fields (Figures 1d–1f) are log-pressure heights taking the scale height as 7 km. There are three maxima in the zonal wind components (Figures 1a and 1d). In December 2001, a double-jet structure was prominent in the upper troposphere over the South Pacific. The enhancement in the westerlies toward 48°S was associated with the entrance region of the higher-latitude jet whose axis was located around 60°S. The maximum at 30°S corresponded to the axis of the lower-latitude jet. The third maximum at 20°S was a strong westerly wind on the northern flank of a cutoff cyclone developing during the period when the observation was being made in the subtropical region.

[11] The crosses in Figures 1a–1c indicate the tropopauses obtained from each of the temperature profiles following the WMO (World Meteorological Organization) standard definition. We can clearly see discontinuity in the tropopause heights. The tropical tropopause is located at an altitude of 17–18 km, while the tropopause to the south of 35°S is located at an altitude of 11–12 km.

[12] It is noteworthy that the ECMWF operational data reproduced a large-scale structure, including easterly winds in the troposphere around the latitude of 35°S, in the middle of the South Pacific, although there were very few upper air observations over a wide longitudinal range. Only eight of our soundings at 10°N, 7°N, 2°S, 4°S, 5°S, 7°S, 21°S, and 44°S were successfully transferred to the Global Telecommunication System (GTS) of WMO. There were, however, some features that were not reproduced. For example, the amplitude of the maximum westerly at 30°S (20 m s^{-1}) was weaker than that in the observations (35 m s^{-1}).

[13] Figure 2 shows synoptic-scale features in the upper troposphere. A double-jet structure could clearly be seen as the jet axes were situated at around 30°S and 60°S. Both jets were meandering because of transient and quasi-stationary disturbances. When observation was conducted in a region from 17°S to 30°S, a cutoff cyclone was moving slowly toward the west in the upper troposphere. When the ship

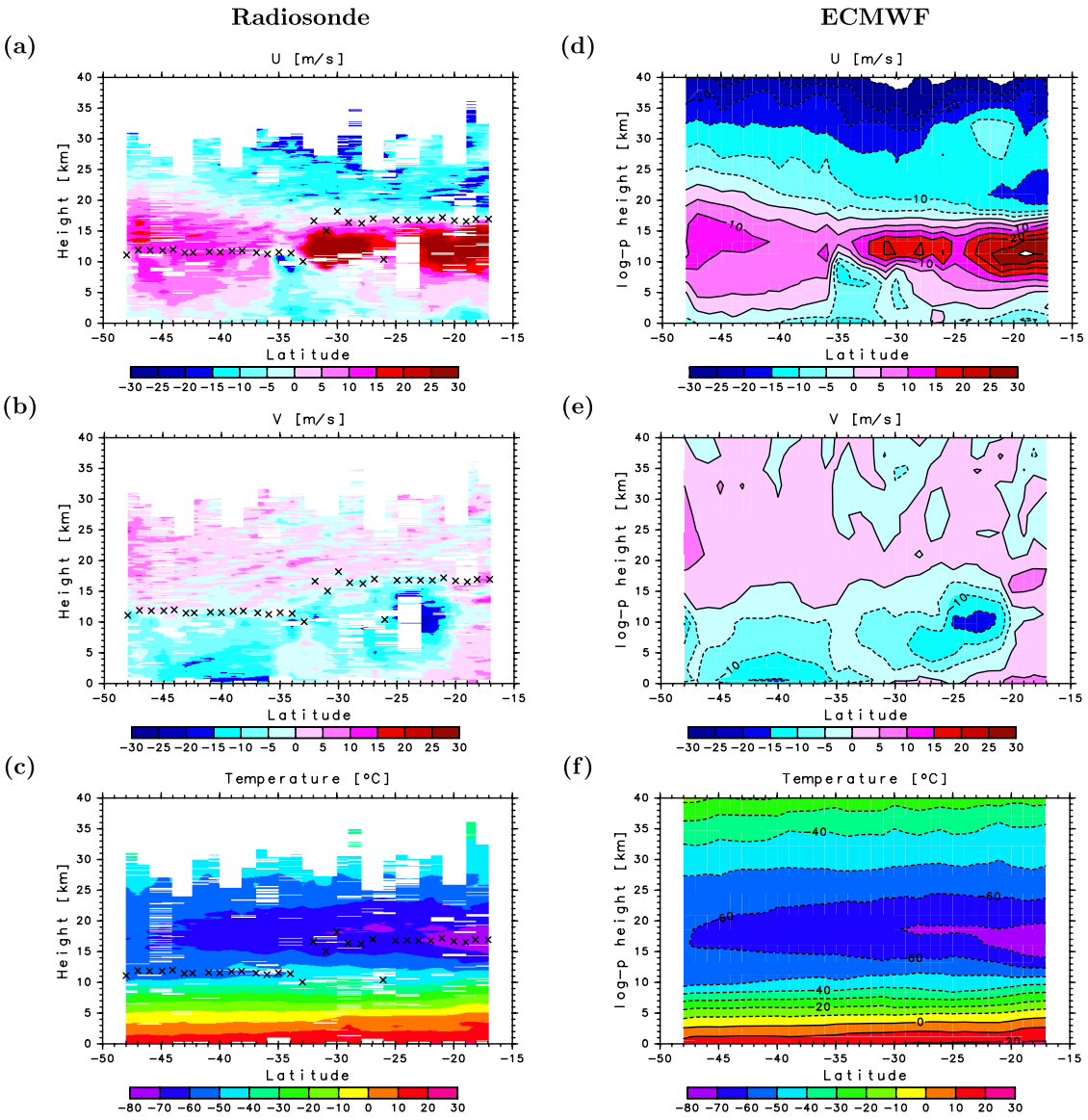

Figure 1. Latitude-height sections of (a and d) zonal and (b and e) meridional winds and (c and f) temperature that were observed with radiosondes (Figures 1a–1c) and were obtained from ECMWF operational analysis (Figures 1d–1f).

reached the midlatitudes, a jet streak embedded in a confluent zone was located to the west of the ship.

3.2. Gravity Wave Field

[14] Previous studies have used various ways of determining gravity wave components from original profiles. *Eckermann and Hocking* [1989] cautioned that the hodograph analysis does not provide accurate estimates of the gravity wave parameters if there exist multiple waves. Moreover, *Zhang et al.* [2004] demonstrated that the derived parameters using hodograph analysis were sensitive to the filter used to separate the wave from a background flow. In this study, we analyzed filtered components extracted with the band-pass filter used for Figure 3, showing vertical profiles of unfiltered and band-pass-filtered zonal and meridional wind and temperature components every 5° in latitude. The cutoff lengths of the band-pass filter were 0.5 and 5 km. This procedure eliminates contributions to the propagation directions from short/long vertical-scale perturbations and statistical noise.

[15] Figure 4 shows the meridional cross sections of kinetic and potential energies per unit mass (KE and PE) of the gravity waves. Note that these sections do not provide representative meridional features of KE and PE since the values at each latitude consist from only one profile. The large values of PE at the midlatitude tropopause are likely due to contamination of the abrupt change of temperature lapse rate and small N^2 that is often observed slightly below the midlatitude tropopause. In other places in the midlatitudes, the PE was at most 2 m^2 s^{-2}. The PE at lower latitudes was larger than that in the midlatitudes. The distribution of KE is rather patchy. The large KE was found in the regions from 32°–34°S around 15 and 20 km, and from 17°–18°S, 25°S, and 30°–33°S in the upper tropo-

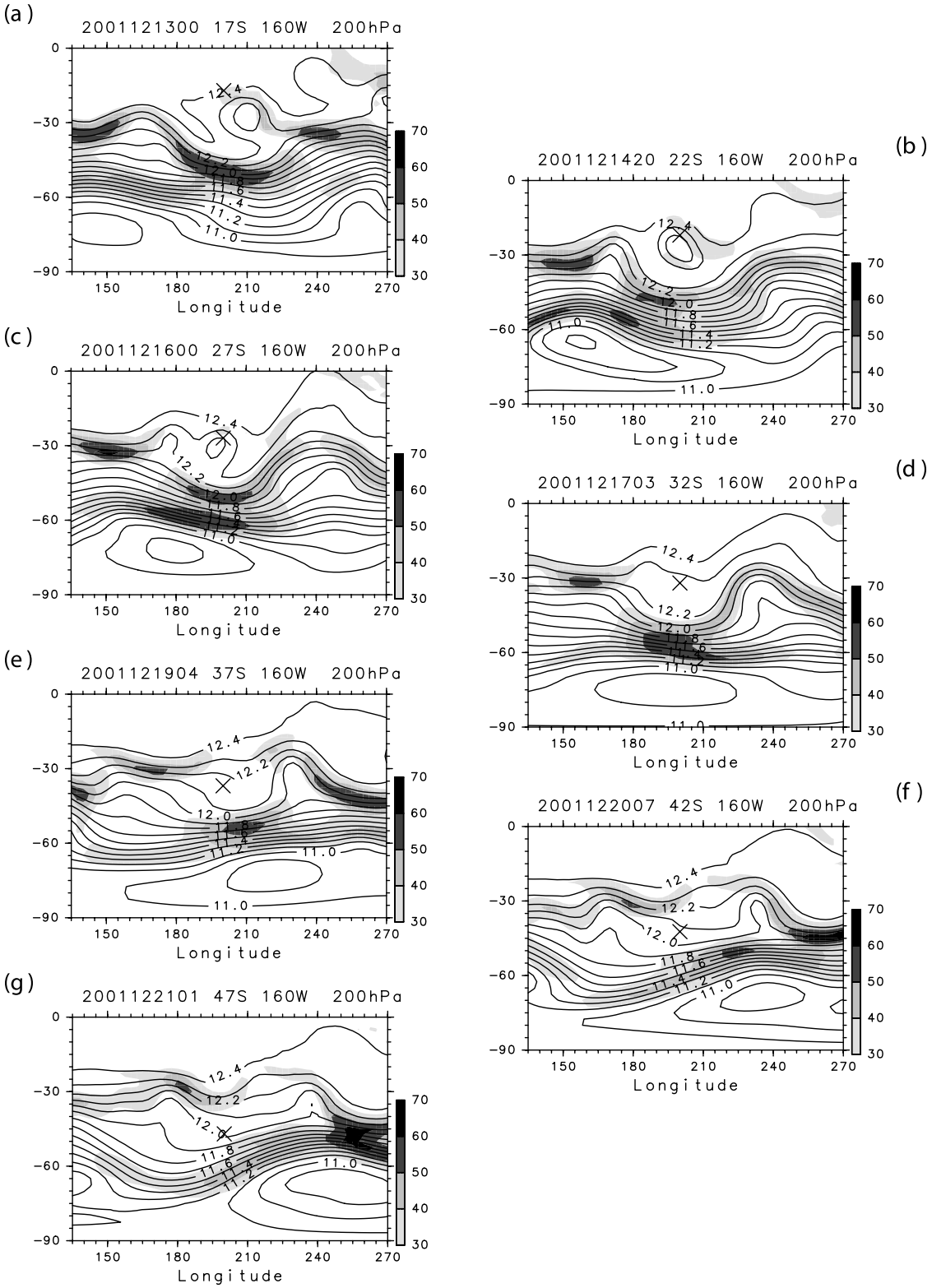

Figure 2. Latitude-longitude sections of geopotential height (in km) at 200 hPa when ship was located at (a) 17°S, (b) 22°S, (c) 27°S, (d) 32°S, (e) 37°S, (f) 42°S, and (g) 47°S. Contour interval is 0.1 km. Shading indicates horizontal wind speed. Crosses show location of ship.

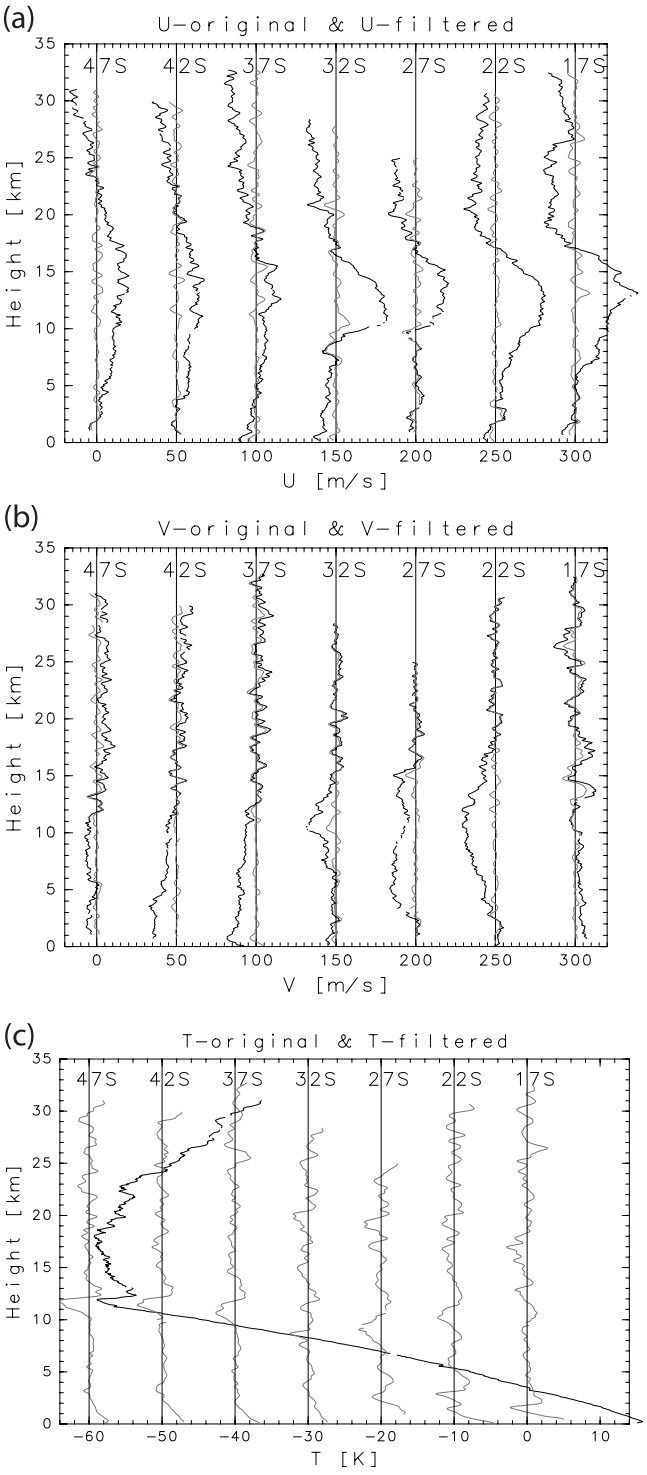

Figure 3. Vertical profiles of unfiltered (black curve) and band-pass-filtered (gray curve) components of (a) zonal and (b) meridional wind and (c) temperature every 5° from 17°S to 47°S. Original profile of temperature only at 47°S is shown. Cutoff vertical wavelengths of band-pass filter are 0.5 and 5 km. Each profile was successively offset by 50 m s^{-1} for clarity.

sphere. The magnitude of KE was about four times that of PE on average, suggesting that low-frequency gravity waves were dominant.

4. Gravity Wave Parameters

[16] Gravity wave parameters were estimated from the sounding data through hodograph analysis and variations in these parameters with latitude and height were evaluated.

4.1. Hodograph Analysis

[17] A hodograph for an inertia gravity wave should be elliptical according to the polarization relation, and the direction of its major axis should indicate the direction of propagation with 180° ambiguity. The ratio of the minor to the major axis equals the ratio of inertial frequency (f) to the intrinsic frequency of wave ($\hat{\omega}$) where the transverse shear effect is negligible [e.g., *Gill*, 1982]. Hodograph analysis has been used for radiosonde data to estimate gravity wave parameters [e.g., *Tsuda et al.*, 1994]. Its advantage is that we can deduce intrinsic frequency from one set of vertical profiles of zonal and meridional winds.

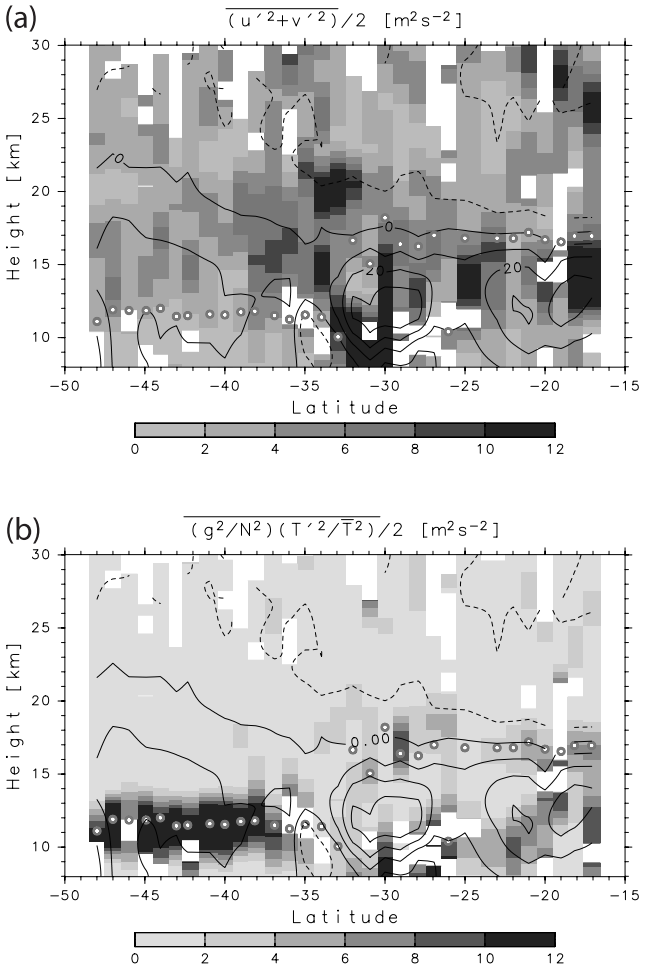

Figure 4. Latitude-height sections of (a) kinetic and (b) potential energies per unit mass of gravity waves. Contours show zonal wind. Interval is 10 m s^{-1}. Negative values are indicated by dashed curves. Circles show height of tropopause.

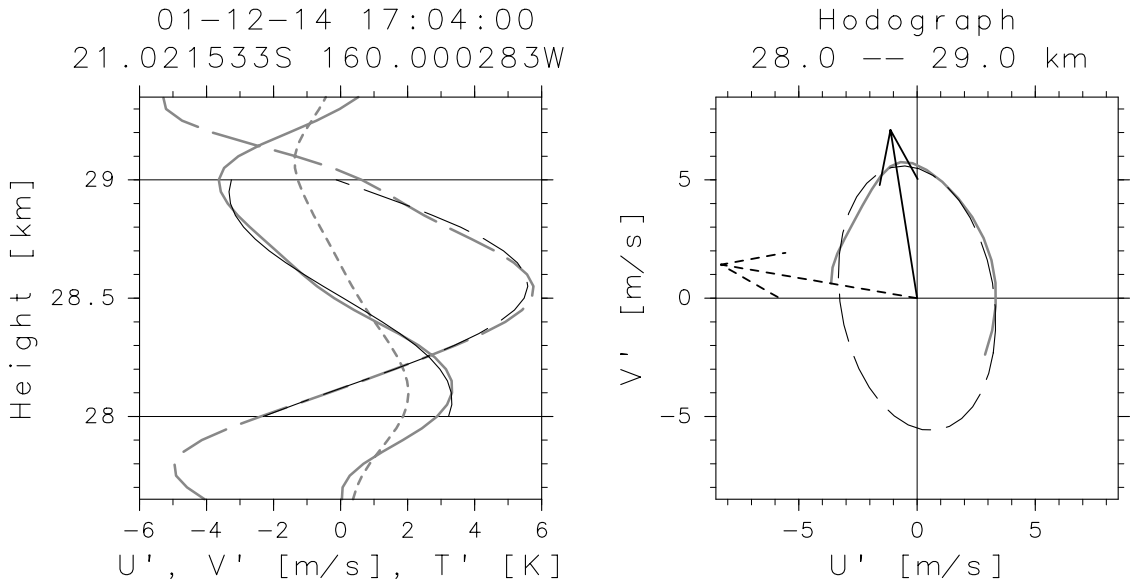

Figure 5. (left) Vertical profiles of zonal (gray solid curve) and meridional wind (gray long-dashed curve) and corresponding fitted curves obtained by least squares fitting to sinusoidal functions (black solid and long-dashed curves) for heights from 28 to 29 km. Temperature fluctuations are also indicated by gray short-dashed curve. (right) Hodograph (gray solid curve) and fitted ellipse (black long-dashed curve). Solid arrow indicates intrinsic phase velocity determined from phase relation between fitted wind component and temperature fluctuations. Short-dashed arrow means background wind.

[18] We obtained the gravity wave parameters with a similar procedure to that used by *Sato and Yamada* [1994]. Examples are shown in Figure 5 and described in what follows. The vertical profiles of zonal and meridional wind components over an analysis height range of 1 km were fitted to sinusoidal curves having a fixed vertical wavelength, using the least squares method. The optimal parameters (vertical wavelength, amplitude, and phase) giving the least residual were determined from 91 fittings having different vertical wavelengths in a range from 0.50 to 5.00 km with an interval of 0.05 km.

[19] Taking $\hat{\omega}$ to be positive without loss of generality, vertical wave number m for upward propagating waves is negative. For the southern hemisphere, negative m indicates counterclockwise rotation of the horizontal wind vector with height. Once m, intrinsic frequency $\hat{\omega}$, and the horizontal propagation direction with an ambiguity of 180° are obtained with the fitting previously described, the magnitude of horizontal wave number vector $\boldsymbol{k_H}$ can be deduced from the dispersion relation

$$\hat{\omega}^2 = f^2 + N^2|\boldsymbol{k_H}|^2/m^2 \tag{1}$$

of inertia gravity waves, giving Brunt-Väisälä frequency N from the average temperature profile.

[20] The ambiguity of direction of the wave number vector obtained from hodograph analysis alone was removed by utilizing temperature data. The horizontal wind component v'_2, which is counterclockwise perpendicular to the direction of propagation, is related to temperature component T' as follows:

$$\frac{T'}{\overline{T}} = -\frac{N^2|\boldsymbol{k_H}|}{mgf} v'_2, \tag{2}$$

where g is the acceleration of gravity and $\overline{T}$ is the background temperature. Thus v'_2 and T' for the upward (downward) propagating waves are anti-phase (in-phase). Accordingly, the cross correlation between v'_2 and T' for the upward (downward) propagating waves were negative (positive). We determined the propagation direction to make the sign for the cross-correlation coefficient between v'_2 and T' consistent.

[21] The calculations of ground-based frequency and ground-based phase velocity require background horizontal winds. In this paper, we took an average of the background (5-km low-pass-filtered) profile over the analysis height range.

[22] In the example in Figure 5, the estimated parameters are as follows: the vertical wavelength is 1.75 km, the horizontal wavelength is 500 km, the intrinsic period is 19 h, the ground-based phase speed is 9.9 m s^{-1}, and the horizontal propagation direction is northward (99° counterclockwise from east).

4.2. Characteristics of Gravity Wave Parameters

[23] We only examined the wave parameters for cases in which the following conditions were satisfied: (1) the variance due to elliptic wind components was larger than twice the residual variance, (2) the ratio of the short to the long axis of horizontal perturbation velocity was greater than 0.05 and less than 0.9 (i.e., $20|f| > \hat{\omega} > 1.1|f|$), (3) the amplitude of horizontal perturbation velocity in the direction of the long axis exceeded 1 m s^{-1}, and (4) the absolute value of the cross-correlation coefficient between v'_2 and T' was larger than 0.3. These conditions are imposed to reject the obtained parameters from vertical profiles where components other than inertia gravity waves seem dominant. The latter of condition (2) are imposed since the horizontal

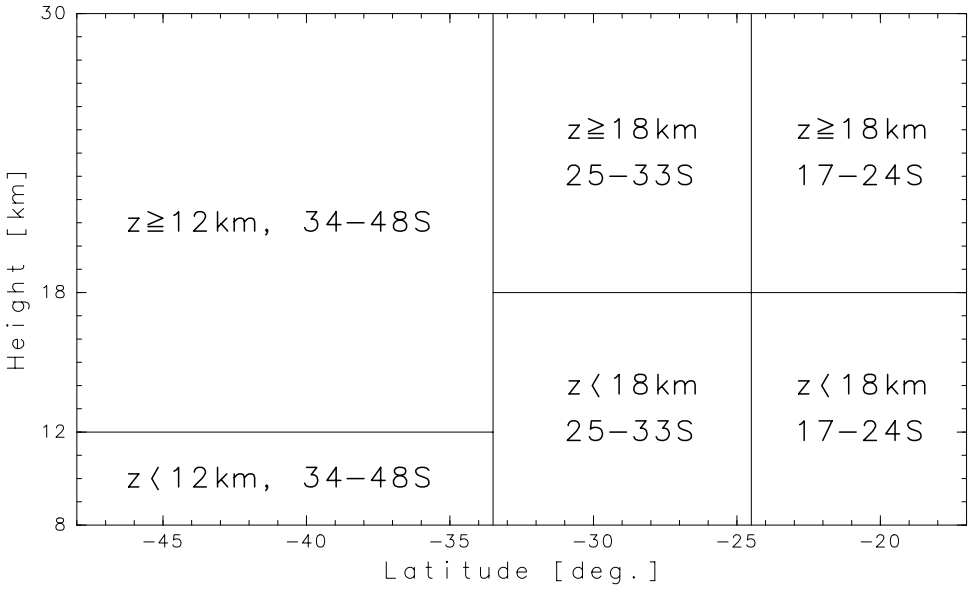

Figure 6. Latitude and height regions for which statistics on gravity wave parameters were prepared.

propagation direction deduced from almost circular hodographs is unreliable.

[24] Statistics of estimated parameters were prepared for each of the six latitude and height regions (shown in Figure 6) with three latitude ranges from 17–24°S, 25–33 °S, and 34–48°S and two height ranges divided by the tropopause (18 km for 17–24°S and 25–33°S, and 12 km for 34–48°S). The boundaries between the regions were determined based on the structure of the background field (Figure 1). Figures 7, 8, 9, and 10 show histograms of estimated horizontal wavelengths, $\hat{\omega}$, $|f/\hat{\omega}|$, and vertical wavelengths, respectively. Medians and averages are also shown in Figures 7–10. We consider the median as a representative value of each parameter in this study since the median is always nearer to the mode than the average.

[25] It is clear that the horizontal wavelengths decrease with increasing latitude south; the median horizontal wavelengths in the stratosphere (troposphere) are 496 (233) km, 270 (214) km, and 255 (92) km for 17°–24°S, 25°–33°S, and 34°–48°S, respectively. For the subtropical (17°–24°S)

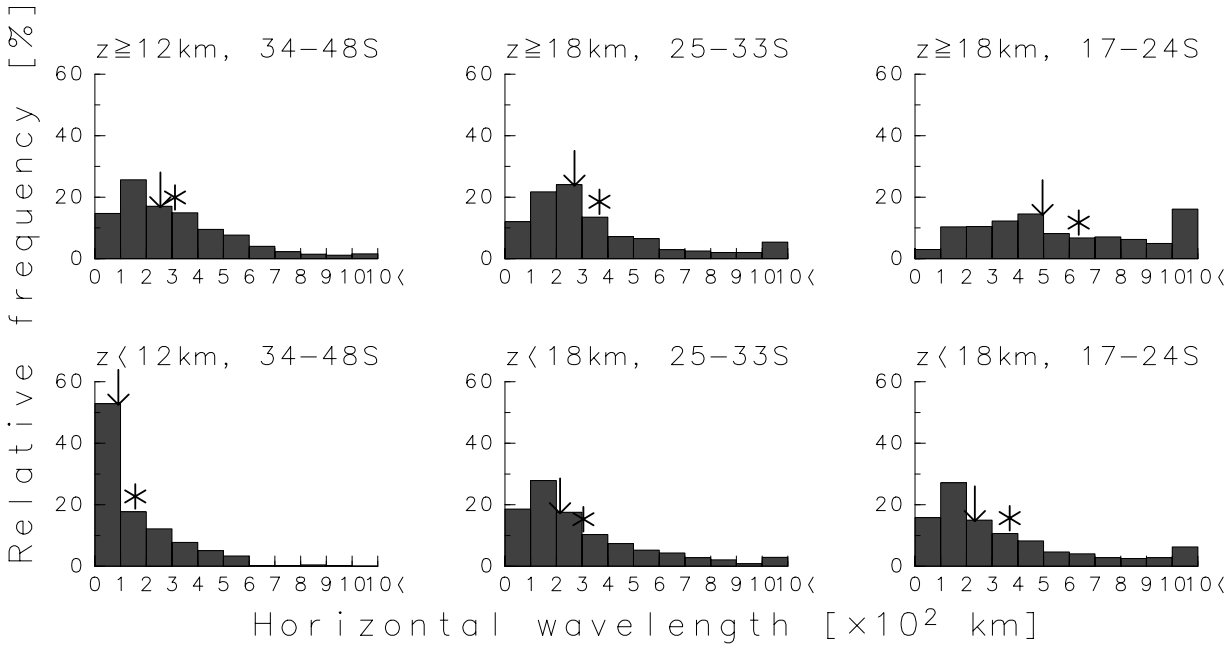

Figure 7. Histograms of horizontal wavelength. Results are presented for latitudes 17°–24°S, 25°–33°S, and 35°–48°S for stratosphere and troposphere respectively. Arrows and asterisks indicate the median and average values.

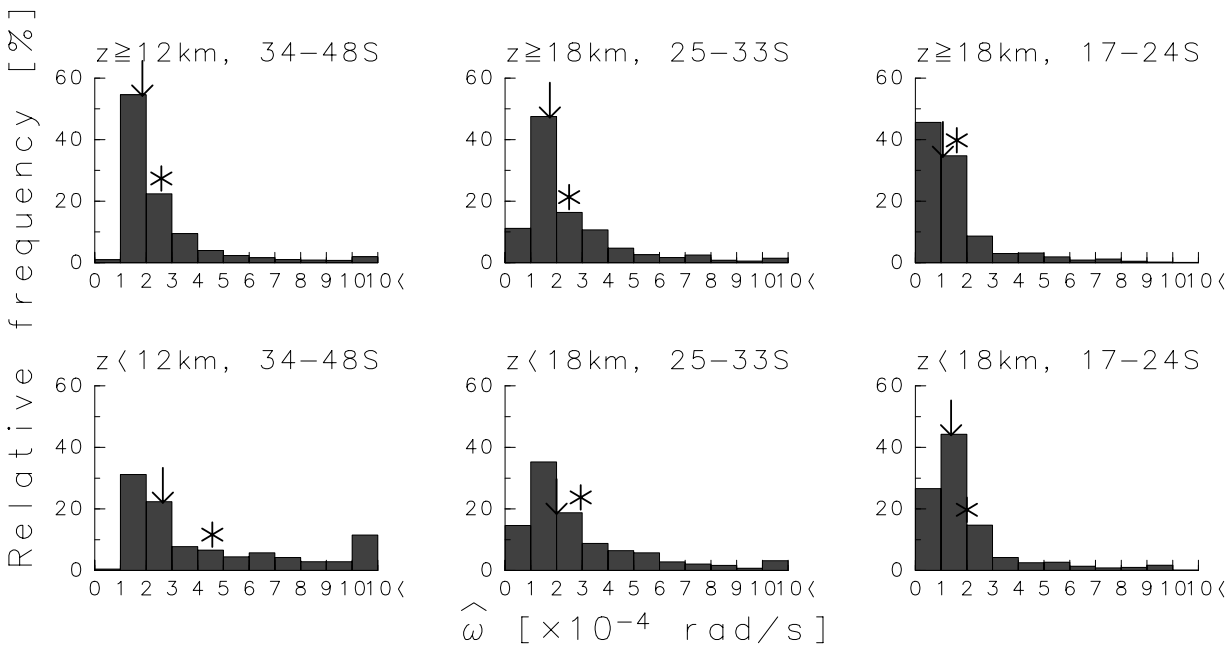

Figure 8. Same as Figure 7 except for intrinsic frequency.

stratosphere, 16% of the waves have horizontal wavelengths longer than 1000 km. The horizontal wavelengths in the stratosphere are longer than those in the troposphere.

[26] The dependence of $\hat{\omega}$ on latitude and height is also significant. The median values increase with increasing latitude for both the stratosphere and troposphere, and those in the troposphere are larger than in the stratosphere. This suggests that the latitudinal variations in $\hat{\omega}$ largely came from f because the values of $f/\hat{\omega}$ do not significantly depend on latitude, especially in the stratosphere. The fraction of values smaller than 0.2 is larger for 25°–33°S and 34°–48°S than for 17°–24°S in the troposphere. The median values are 0.5 and 0.3 for the stratosphere and troposphere for all latitude ranges. Especially, the distributions for $f/\hat{\omega}$ in the stratosphere are remarkably similar among latitudes.

[27] The dominant vertical wavelengths in the stratosphere are 1–2 km for all latitude ranges. The dependence on latitude is not clear. The median vertical wavelengths in the troposphere are 2–3 km and larger than those in the stratosphere. The dominant vertical wavelengths for downward propagating waves are 4–5 km except for the midlat-

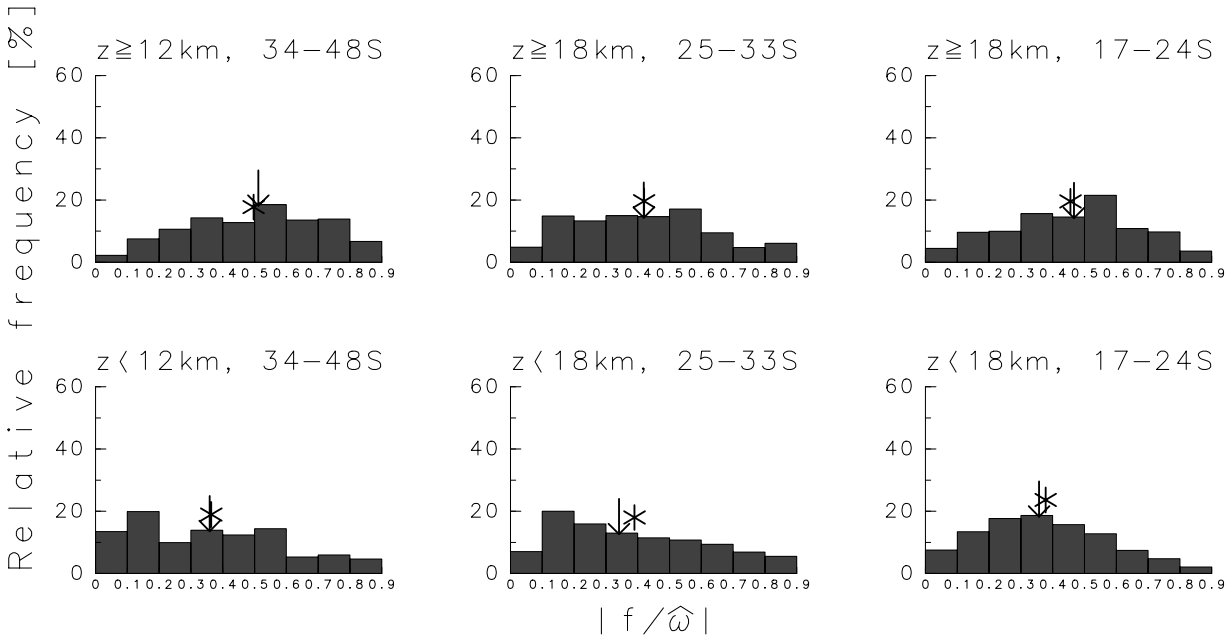

Figure 9. Same as Figure 7 except for $|f/\hat{\omega}|$.

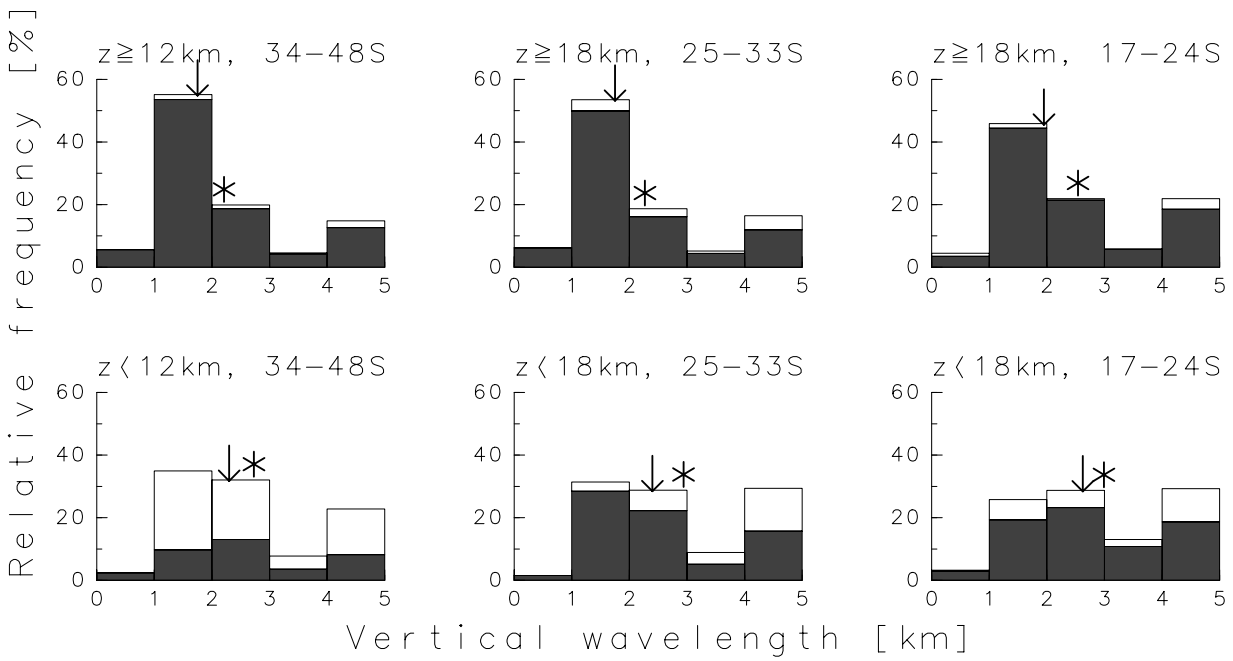

Figure 10. Stacked histograms of vertical wavelength. The contributions of upward and downward propagation are indicated by solid and open columns, respectively.

itude troposphere, where downward propagating waves with wavelengths less than 3 km are dominant.

5. Propagation Properties of Gravity Waves

[28] As can be seen from Figure 10, about 90% of waves propagated upward in the stratosphere. The fractions for upward propagation in the troposphere were 75, 73, and 35% for 17°–24°S, 25°–33°S, and 34°–48°S, respectively.

[29] Figure 11a shows horizontal phase velocities relative to the ground in the meridional section. Each arrow indicates the horizontal phase velocity vector; rightward and downward in the paper plane indicate northward and eastward, respectively. The type of line for each arrow (solid or dashed) indicates the vertical propagation direction (upward or downward), respectively. The starting point for each arrow is placed at the middle of the height range to which hodograph analysis was applied. Figure 11b shows a similar section but for meridional and vertical components of group velocity.

[30] Downward energy propagation mainly appears below the strong westerlies over latitudes from 20 to 33°S. In particular, downward propagating waves around 30°–33°S and 10 km had a large kinetic energy. Almost all the waves propagated upward in the other places. Southward propagation is more dominant than northward propagation. Notable northward propagation is only found around 21°–23°S above 22 km and 37°S around 20 km. To the south of 37°S, almost all waves propagated southward.

[31] Figure 12 plots the relative frequency distributions for ground-based phase velocities of gravity waves observed in the stratosphere and troposphere classified according to both direction and magnitude. The most dominant direction is southward in the stratosphere, with a little bias southeastward for latitudes 34°–48°S. The relative frequency where the propagation direction was between 120° and 210° clockwise from the north was 44%. A preference for southward propagation can also be seen for latitudes 25°–33°S. However, the most preferred propagation direction for latitudes 17°–24°S is northward. Eastward and westward propagation are suppressed compared with the other latitude regions. Northward propagating waves will be examined in section 6.

[32] Eastward propagation in the troposphere is more dominant for latitudes 25°–33°S and 34°–48°S than in the stratosphere. However, southward propagation is most dominant for latitudes 17°–24°S.

6. Discussion

6.1. Comparison of Gravity Wave Parameters With Northern Hemisphere Statistics

[33] Previous studies have obtained statistics regarding gravity wave parameters in the northern hemisphere landmasses. *Sato* [1994] presented histograms of gravity wave parameters and the horizontal propagation direction in the stratosphere using wind data observed with the MU radar at Shigaraki, Japan (35°N, 136°E) in 1986–1988. The average vertical wavelength, horizontal wavelength, and $f/\hat{\omega}$ for the summer stratosphere were 1.6 km, 300 km, and 0.54, respectively, which were remarkably close to our results (1.75 km, 270 km, and 0.51). The preferred direction was poleward for the summer stratosphere, which is similar to our statistics for the midlatitude stratosphere. *Sato* [1994, Figure 12b] indicates that the poleward propagation is dominant in the lower stratosphere regardless of the relative position of the observation to the subtropical jet. The characteristics are also seen in Figure 11.

[34] *Wang et al.* [2005] presented 5-year statistics of gravity wave parameters derived from radiosonde data at 94 U. S. stations. They found a clear dependence of horizontal wavelengths on latitude and height and depen-

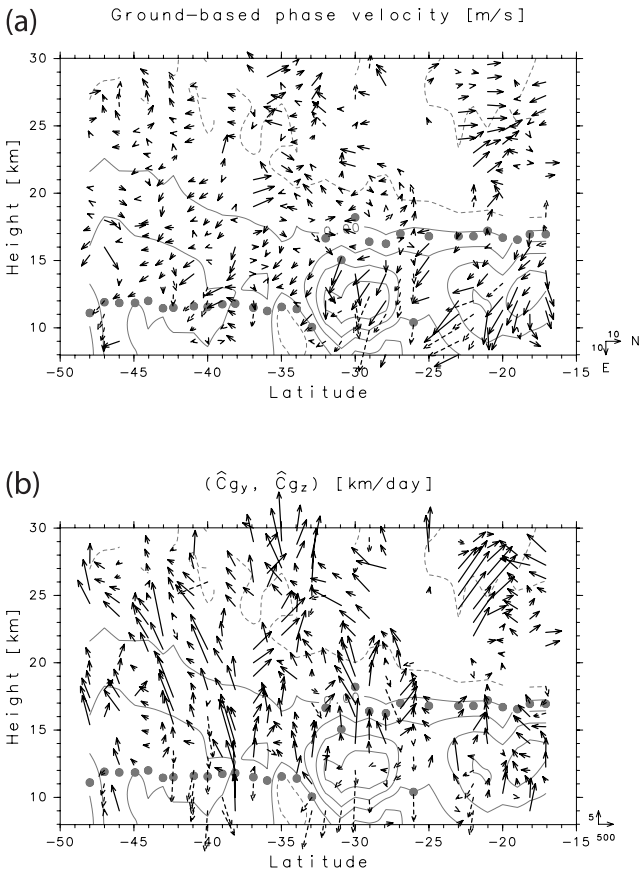

Figure 11. Latitude-height sections of (a) horizontal phase velocities relative to ground and (b) meridional and vertical components of group velocity. Rightward and downward arrows at bottom right in Figure 11a show northward and eastward phase velocities of 10 m s^{-1}, respectively. Upward and rightward arrows at bottom right in Figure 11b show upward component of 5 km d^{-1} and northward component of 500 km d^{-1}, respectively. Solid and dashed arrows in Figures 11a and 11b indicate upward and downward energy propagation, respectively. Contours show zonal wind. Interval is 10 m s^{-1}. Negative values are indicated by dashed curves. Closed circles show height of tropopause.

dence of vertical wavelengths on height, which is similar to our results. The dependence of $\hat{\omega}/f$ on height is also similar to our results, although the averaged values of $\hat{\omega}/f$ in June–August (2.7–2.9 and 3.9 for the lower stratosphere and troposphere respectively) are 20–30% greater than our results (2.0–2.4 and 2.8–2.9). The dependence of vertical wavelengths on latitude found by *Wang et al.* [2005] was not clear from our results both in the troposphere and stratosphere. However, it is clear from *Wang et al.* [2005, Figure 3] that the vertical wavelengths in the troposphere over the eastern U. S. exhibit no dependence on latitude. Our result for the troposphere over oceanic regions is consistent with their result for the troposphere over relatively flat landmasses. The dependence of vertical wavelengths on height is also clear in our results.

6.2. Distribution of KE and PE

[35] The global distributions of gravity waves in terms of PE based on GPS occultation temperature profiles were discussed by *Tsuda et al.* [2000]. According to their Plate 1, the PE averaged within a range of 20–30 km in the same region we examined was estimated to be 1.5–3.0 m^2 s^{-2}. Our results were less than their estimates and 1.2 m^2 s^{-2} on average.

[36] Figure 4 indicates that KE is often three times larger than PE and the distribution for KE is considerably different from that for PE. The partitioning of total gravity wave energy into PE and KE depends on the aspect ratio $\alpha \equiv |\boldsymbol{k_H}|/|m|$ [*Gill*, 1982]:

$$\frac{KE}{PE} = 1 + \frac{2f^2}{N^2\alpha^2}. \tag{3}$$

The ratio $f/\hat{\omega}$ is also related to α as

$$\frac{\hat{\omega}^2}{f^2} = 1 + \frac{N^2\alpha^2}{f^2}. \tag{4}$$

Eliminating α from Equations (3) and (4) yields

$$\frac{KE}{PE} = \frac{1 + (f/\hat{\omega})^2}{1 - (f/\hat{\omega})^2}. \tag{5}$$

Thus low-frequency gravity waves with large $|f/\hat{\omega}|$ have a large KE/PE ratio. The large value for KE/PE is consistent with the dominance of low-frequency gravity waves as shown in Figure 9. The dominance of gravity waves with near-inertial frequency was reported by both observational and GCM-based studies [e.g., *Vincent et al.*, 1997; *Sato et al.*, 1999; *Hertzog et al.*, 2002]. It is interesting that such waves were observed at various latitudes. It should simultaneously be noted that the hodograph analysis tends to emphasize low-frequency waves. This is because they are the clearest signature in an hodograph, and because their propagation away from sources is slowest [*Alexander et al.*, 2002].

6.3. Source Detection by Ray-Tracing Analysis

[37] Ray-tracing analysis was done to find the sources of southeastward propagating gravity waves which are dominant in 34°–48°S in the stratosphere and those propagating northward in the subtropics. Details on the integration of rays are described in Appendix A.

6.3.1. Source of Southeastward Propagating Waves

[38] As can be seen from Figure 12, the most dominant direction was southeastward. This feature was more prominent in the midlatitude stratosphere.

[39] Figure 13 is a histogram of the heights of the final points of rays calculated for gravity waves with a southeastward phase velocity in the midlatitude stratosphere. Fifty percent of the final points are located within 9–14 km. This suggests that the gravity waves were generated in the vicinity of the jet stream. As noted from Figure 2, the higher- and lower-latitude jets always meandered and often joined during the observation period. It is likely that gravity waves were continuously radiated from around the fluctuating jet.

6.3.2. Source of Northward Propagating Waves in the Subtropics

[40] Notable northward and upward propagation was found around 23°S in the lower stratosphere. The most

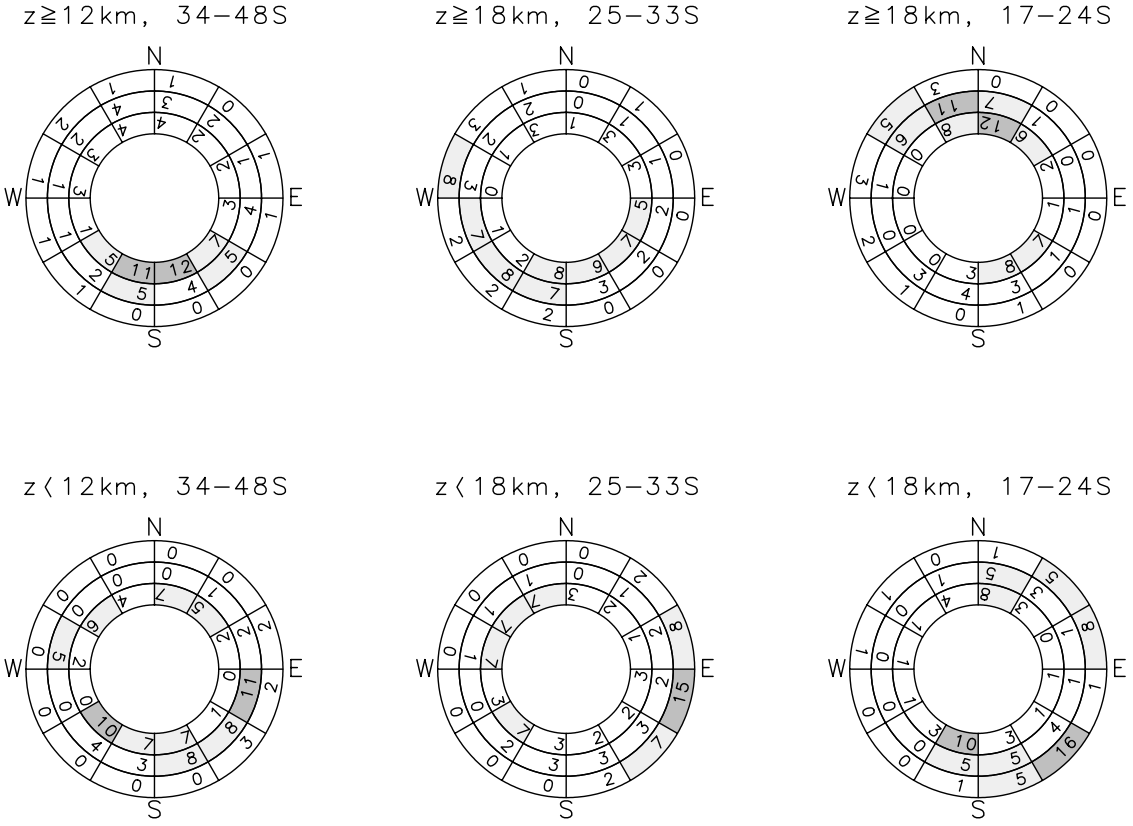

Figure 12. Relative frequency distribution of ground-based phase velocities in stratosphere and troposphere for three latitudinal ranges of 17°–24°S, 25°–33°S, and 34°–48°S. Horizontal phase velocities were binned into a histogram according to direction and magnitude. Relative frequency of waves with phase speeds of 0–10, 10–20, and larger than 20 m s^{-1} in terms of percentages are shown in inner, middle, and outer rings, respectively. Segments more than 5% and 10% are lightly and darkly shaded, respectively.

striking feature in the upper troposphere in the subtropics during the observation period was a cutoff cyclone which developed around 30°S. The cutoff cyclone was formed at 2000 UTC 11 December around 145°W, 28°S as can be noted from the closed contours of the geopotential height on isobaric surfaces between 200 and 500 hPa, when we made an observation at 11°S. The cutoff cyclone slowly moved westward and continued to develop till 0800 UTC 15 December. At that time, the research vessel was located at 25°S and was closest to the center of the cyclone (Figure 2). After that, the cyclone began to dissipate. The local Rossby number ($Ro \equiv |\zeta/f|$) calculated with the ECMWF operational analysis data exceeded one around the peak stage of the cyclone.

[41] Figure 14 shows three backward rays starting from 29.05 km and 29.05 ± 0.05 km at 160°W and 23°S. Initial values of wave parameters were as those estimated from vertical profiles for heights 0.05 km below and above the starting point. The rays have been drawn on three orthogonal projection planes. The horizontal distribution of geopotential height and *Ro* at 150 hPa are also shown. It is clear that the rays are traced back not to the exact maximum of *Ro* but to the vicinity of the center of the cutoff cyclone where *Ro* is enhanced. The results strongly suggest that gravity waves were generated near the cutoff cyclone.

[42] Since the ray equations are strictly valid in the far field away from the source region, it is difficult to describe exact wave parameters at the source. The calculated parameters, however, include information of the characteristics of the wave at the supposed sources. For the case of the ray

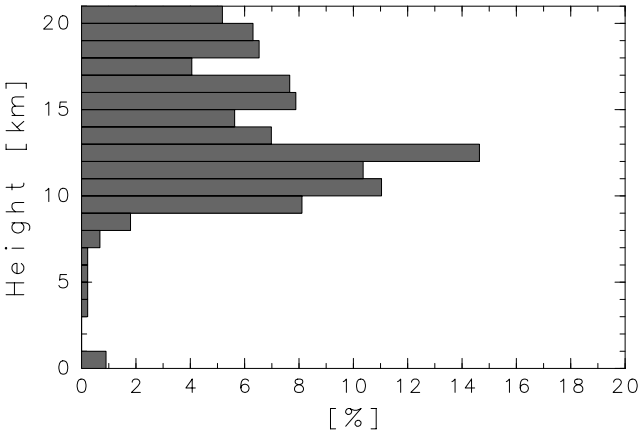

Figure 13. Relative frequency distribution of final points of rays for southeastward propagating waves observed above 18 km.

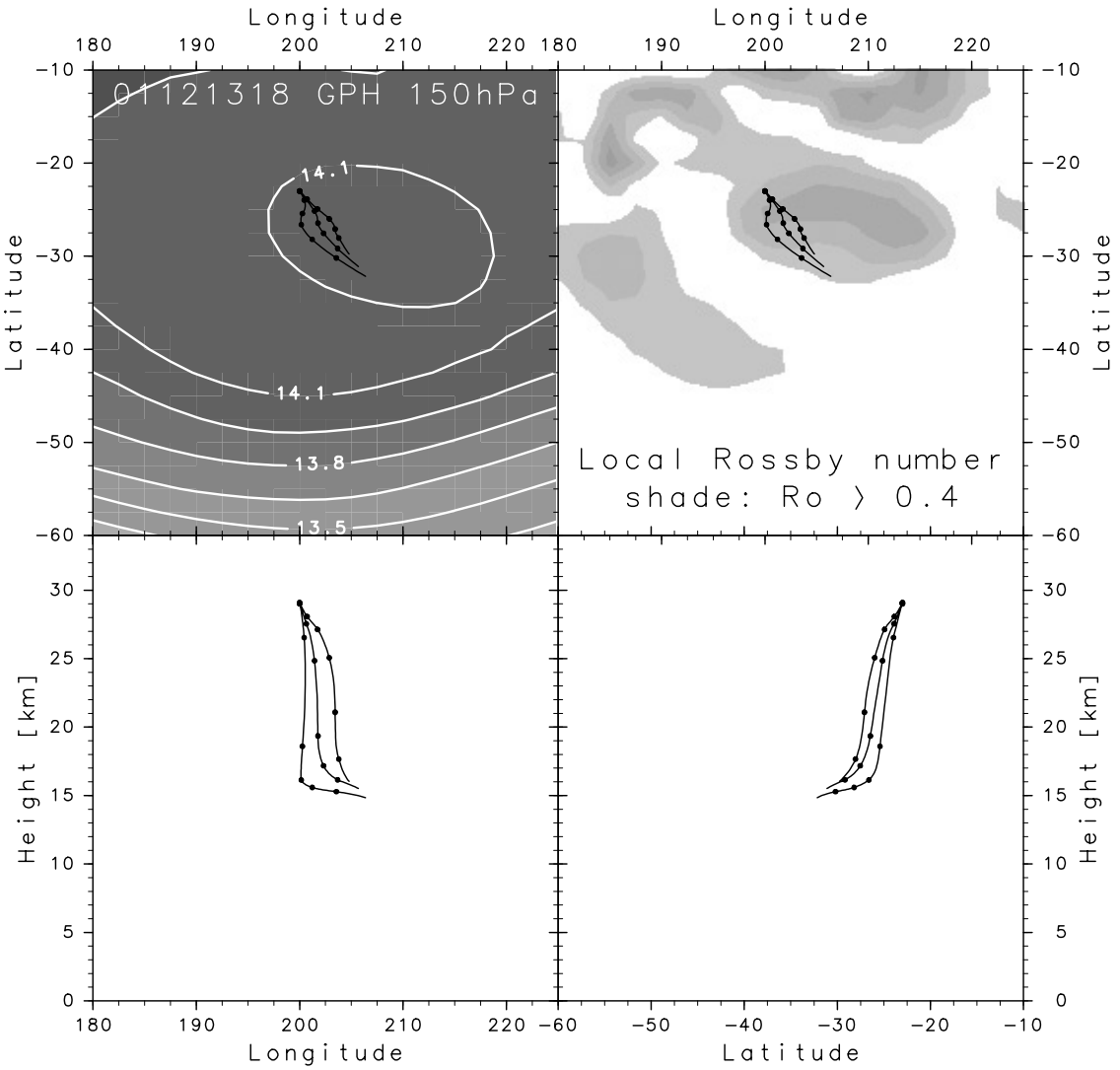

Figure 14. Rays integrated backward in time (solid black curves) for 30 hours from 0000 UTC 15 December and (160°W, 23°S, 29.05 ± 0.05 km) in (top left) longitude-latitude, (bottom left) longitude-height, and (bottom right) latitude-height sections. Solid circles on the rays indicate the positions every 6 hours from the starting points. Shading and white contours indicate geopotential height at 150 hPa at 1800 UTC 13 December. (top right) Horizontal distribution of local Rossby number at the same pressure level and time. Shading intervals for geopotential height and *Ro* are 0.15 km and 0.2, respectively.

starting from 29.05 km altitude, the horizontal and vertical wavelengths of 200 km and 1.95 km decrease to 185 km and 1.70 km, respectively, during 30 hours of backward integration.

7. Summary and Concluding Remarks

[43] Using the horizontal winds and temperature data obtained by radiosondes at intervals of 1° in a latitudinal range of 17°–48°S along 160°W during a cruise experiment, we first described the characteristics of inertia gravity waves over the subtropical and extratropical South Pacific. Gravity wave parameters were estimated by hodograph analysis.

[44] The statistics on these parameters were compiled for each section bounded by latitude (17°–24°S, 25°–33°S, and 34°–48°S) and height (18 km for 17°–24°S and 25°–33°S, and 12 km for 34°–48°S). The dominant horizontal wavelengths decreased with increasing latitude, with larger values in the lower stratosphere. The Coriolis parameter f divided by $\hat{\omega}$ was ~0.5 in the lower stratosphere and ~0.3 in the troposphere, with little dependence on latitude. The dominant vertical wavelengths for upward propagating waves were 1–2 km in the lower stratosphere and 2–3 km in the troposphere. The dependence of vertical wavelengths on latitude was not clear.

[45] The statistics on ground-based phase velocity were also obtained in terms of both direction and magnitude. Southward propagation was dominant in the stratosphere in the midlatitudes while northward propagation was significant in the lower latitudes. The fraction of eastward propagation was enhanced in the troposphere.

[46] Sources of these gravity waves were discussed for two distinctive cases on the basis of ray-tracing analysis. The meandering jet in the upper troposphere was estimated

to be the major source of southeastward propagating gravity waves in the stratosphere. The source of northward propagating waves found in the subtropical lower stratosphere was estimated to be a developing cutoff cyclone through ray tracing.

[47] Several differences and similarities were found between previous northern hemispheric statistics and our results. The gravity wave parameters obtained with the MU radar [*Sato*, 1994] (horizontal wavelengths of 300 km and $f/\hat{\omega}$ of 0.54) are remarkably similar to our results (270 km and 0.51). It is important to accumulate observations over the oceanic region to construct robust statistics for gravity waves. Such observations are also important for evaluating the gravity wave field obtained by very high resolution GCMs, which have recently been developed.

Appendix A: Ray-Tracing Analysis

[48] A "ray" is defined as the trajectory of a point moving at the local group velocity depending on the wave parameters, position, and time:

$$\frac{d_g \boldsymbol{X}(t)}{dt} = \boldsymbol{C}_g[\boldsymbol{k}(\boldsymbol{X}(t)), \boldsymbol{X}(t), t] \tag{A1}$$

$$\omega = \Delta(\boldsymbol{k}, \boldsymbol{X}, t) \tag{A2}$$

$$\boldsymbol{C}_g(\boldsymbol{k}, \boldsymbol{X}, t) = \left(\frac{\partial \Delta}{\partial k}, \frac{\partial \Delta}{\partial l}, \frac{\partial \Delta}{\partial m}\right) \tag{A3}$$

$$\left(\frac{\partial}{\partial t} + \boldsymbol{C}_g \cdot \nabla\right) \equiv \frac{d_g}{dt}. \tag{A4}$$

Wave parameters vary in propagating through nonuniform and/or nonstationary background fields. Under WKBJ approximation and for inertia gravity waves [*Andrews et al.*, 1987; *Oshima*, 1997], the temporal evolution of wave parameters can be written as

$$\frac{d_g X}{dt} = -\frac{k(N^2 - \hat{\omega}^2)}{\hat{\omega}(k^2 + l^2 + m^2)} + U \tag{A5}$$

$$\frac{d_g Y}{dt} = -\frac{l(N^2 - \hat{\omega}^2)}{\hat{\omega}(k^2 + l^2 + m^2)} + V \tag{A6}$$

$$\frac{d_g Z}{dt} = -\frac{m(N^2 - \hat{\omega}^2)}{\hat{\omega}(k^2 + l^2 + m^2)} \tag{A7}$$

$$\frac{d_g k}{dt} = -\frac{(k^2 + l^2)(N^2)_x}{2\hat{\omega}(k^2 + l^2 + m^2)} - kU_x - lV_x \tag{A8}$$

$$\frac{d_g l}{dt} = -\frac{(k^2 + l^2)(N^2)_y + 2m^2 f\beta}{2\hat{\omega}(k^2 + l^2 + m^2)} - kU_y - lV_y \tag{A9}$$

$$\frac{d_g m}{dt} = -\frac{(k^2 + l^2)(N^2)_z}{2\hat{\omega}(k^2 + l^2 + m^2)} - kU_z - lV_z \tag{A10}$$

$$\hat{\omega}^2 = f^2 + N^2|\mathrm{k}|^2/m^2. \tag{A11}$$

[49] The initial values of (k, l, m, ω) were those estimated by hodograph analysis described in section 4. Background information N^2, U, and V at the point of the wave packet was obtained by linear interpolation of the ECMWF operational analysis data in latitude, longitude and log-p height (taking the scale height as 7 km), and cubic-spline interpolation in time. The numerical integration used was the fourth-order Runge-Kutta method. The time step was taken to be 30 min.

[50] We continued each time integration for 5 days unless any of these conditions were satisfied: (1) $\hat{\omega} < |f|$, (2) $\hat{\omega} > N$, (3) $\delta \equiv |dm/dz|/m^2 \sim |dm/dt|/(C_{g_z} m^2) \mid \gg 1$ [*Marks and Eckermann*, 1995], and (4) ray reached below 1000 hPa or above 1 hPa. Of 6361 calculations, 44%, 0%, 52%, and 4% were ended because of the satisfaction of conditions 1, 2, 3, and 4, respectively.

[51] **Acknowledgments.** The MeSSO2001 experiment was performed by S. Ogino, N. Takahashi, Y. Tomikawa, and T. Yamanouchi together with the authors. The authors wish to thank I. Koike and M. Terazaki, the Principal Investigators of the Hakuho-maru research cruise, for their having given us the opportunity to do this experiment. We greatly appreciate the cooperation and encouragement given by the crew of the Hakuho-maru throughout the cruise. We acknowledge the support of R. Kimura, H. Niino, K. Ishikawa and their students in performing this experiment. The ray-tracing calculation in the present paper was based on the parcel trajectory calculation program developed by *Tomikawa and Sato* [2005]. The authors would like to thank M. Takahashi, Y. Kawatani, I. Hirota, the editor J. Austin, and three anonymous reviewers for their constructive comments and suggestions. One of the authors (MY) also thanks S. K. Dhaka and S. Yoden for their valuable comments. Most of this work was conducted when one of the authors (MY) was with the Center for Climate System Research of the University of Tokyo.

[52] This research was supported by a Grant-in-Aid for Scientific Research (B)(2) 12440126 made by the Ministry of Education, Culture, Sports, Science and Technology of Japan.

References

Alexander, M. J., and T. J. Dunkerton (1999), A spectral parameterization of mean-flow forcing due to breaking gravity waves, *J. Atmos. Sci.*, *56*, 4167–4182.

Alexander, M. J., T. Tsuda, and R. A. Vincent (2002), Latitudinal variations observed in gravity waves with short vertical wavelengths, *J. Atmos. Sci.*, *59*, 1394–1404.

Allen, S. J., and R. A. Vincent (1995), Gravity wave activity in the lower atmosphere: Seasonal and latitudinal variations, *J. Geophys. Res.*, *100*(D1), 1327–1350.

Andrews, D. G., J. R. Holton, and C. B. Leovy (1987), *Middle Atmosphere Dynamics*, 489 pp., Elsevier, New York.

Chane-Ming, F., G. Roff, L. Robert, and J. Leveau (2002), Gravity wave characteristics over Tromelin Island during the passage of cyclone Hudah, *Geophys. Res. Lett.*, *29*(6), 1094, doi:10.1029/2001GL013286.

Eckermann, S. D., and W. Hocking (1989), The effect of superposition on measurements of atmospheric gravity waves: A cautionary note and some re-interpretations, *J. Geophys. Res.*, *94*(D5), 6333–6339.

Gill, A. E. (1982), *Atmosphere-Ocean Dynamics*, 662 pp., Elsevier, New York.

Guest, F. M., M. J. Reeder, C. J. Marks, and D. J. Karoly (2000), Inertia-gravity waves observed in the lower stratosphere over Macquarie Island, *J. Atmos. Sci.*, *57*, 737–752.

Hertzog, A., F. Vial, C. R. Mechoso, C. Basdevant, and P. Cocquerez (2002), Quasi-Lagrangian measurements in the lower stratosphere reveal an energy peak associated with near-inertial waves, *Geophys. Res. Lett.*, *29*(8), 1229, doi:10.1029/2001GL014083.

Hines, C. O. (1997), Doppler-spread parameterization of gravity-wave momentum deposition in the middle atmosphere. 1. Basic formulation, *J. Atmos. Terr. Phys.*, *59*, 371–386.

Iwasaki, T., S. Yamada, and K. Tada (1989), A parameterization scheme of orographic gravity wave drag with two different vertical partitionings part I: Impacts on medium-range forecasts, *J. Meteorol. Soc. Jpn.*, *67*(1), 11–27.

Kitamura, Y., and I. Hirota (1989), Small-scale disturbances in the lower stratosphere revealed by daily rawinsonde observations, *J. Meteorol. Soc. Jpn.*, *67*(5), 817–831.

Manzini, E., N. A. McFarlane, and C. McLandress (1997), Impact of the Doppler spread parameterization on the simulation of the middle atmosphere circulation using the MA/ECHAM4 general circulation model, *J. Geophys. Res.*, *102*(D22), 25,751–25,762.

Marks, C. J., and S. D. Eckermann (1995), A three-dimensional nonhydrostatic ray-tracing model for gravity waves: Formulation and preliminary results for the middle atmosphere, *J. Atmos. Sci.*, *52*, 1959–1984.

McFarlane, N. A. (1987), The effect of orographically excited gravity-wave drag on the general-circulation of the lower stratosphere and troposphere, *J. Atmos. Sci.*, *44*, 1775–1800.

Oshima, R. (1997), Ray tracing analyses of gravity waves observed by MU radar, MS thesis, Kyoto Univ., Kyoto, Japan.

Palmer, T. N., G. J. Shutts, and R. Swinbank (1986), Alleviation of a systematic westerly bias in general circulation and numerical weather prediction models through an orographic gravity wave drag parameterization, *Q. J. R. Meteorol. Soc.*, *112*, 1001–1040.

Plougonven, R., H. Teitelbaum, and V. Zeitlin (2003), Inertia gravity wave generation by the tropospheric midlatitude jet as given by the Fronts and Atlantic Storm-Track Experiment radio soundings, *J. Geophys. Res.*, *108*(D21), 4686, doi:10.1029/2003JD003535.

Rocken, C., et al. (1997), Analysis and validation of GPS/MET data in the neutral atmosphere, *J. Geophys. Res.*, *102*(D25), 29,849–29,866.

Sato, K. (1994), A statistical study of the structure, saturation and sources of inertio-gravity waves in the lower stratosphere observed with the MU radar, *J. Atmos. Terr. Phys.*, *56*, 755–774.

Sato, K., and M. Yamada (1994), Vertical structure of atmospheric gravity waves revealed by the wavelet analysis, *J. Geophys. Res.*, *99*(D22), 20,623–20,631.

Sato, K., T. Kumakura, and M. Takahashi (1999), Gravity waves appearing in a high-resolution GCM simulation, *J. Atmos. Sci.*, *56*, 1005–1018.

Sato, K., M. Yamamori, S. Ogino, N. Takahashi, Y. Tomikawa, and T. Yamanouchi (2003), A meridional scan of the stratospheric gravity wave field over the ocean in 2001 (MeSSO2001), *J. Geophys. Res.*, *108*(D16), 4491, doi:10.1029/2002JD003219.

Tomikawa, Y., and K. Sato (2005), Design of the NIPR trajectory model, *Polar Meteorol. Glaciol.*, *19*, 120–137.

Tsuda, T., Y. Murayama, H. Wiryosumarto, S. Harijono, and S. Kato (1994), Radiosonde observations of equatorial atmosphere dynamics over Indonesia: 2. Characteristics of gravity-waves, *J. Geophys. Res.*, *99*(D4), 10,507–10,516.

Tsuda, T., M. Nishida, C. Rocken, and R. H. Ware (2000), A global morphology of gravity wave activity in the stratosphere revealed by the GPS occultation data (GPS/MET), *J. Geophys. Res.*, *105*(D6), 7257–7274.

Vincent, R. A., and M. J. Alexander (2000), Gravity waves in the tropical lower stratosphere: An observational study of seasonal and interannual variability, *J. Geophys. Res.*, *105*(D14), 17,971–17,982.

Vincent, R. A., S. J. Allen, and S. D. Eckermann (1997), Gravity wave parameters in the lower stratosphere, in *Gravity Wave Processes: Their Parameterization in Global Climate Models*, edited by K. Hamilton, pp. 7–25, Springer, New York.

Wang, L., M. A. Geller, and M. J. Alexander (2005), Spatial and temporal variations of gravity wave parameters. part I: Intrinsic frequency, wavelength, and vertical propagation direction, *J. Atmos. Sci.*, *62*, 125–142.

Ware, R., et al. (1996), GPS sounding of the atmosphere from low Earth orbit: Preliminary results, *Bull. Am. Meteorol. Soc.*, *77*, 19–40.

Warner, C. D., and M. E. McIntyre (2001), An ultrasimple spectral parameterization for nonorographic gravity waves, *J. Atmos. Sci.*, *58*, 1837–1857.

Wilson, R., M. L. Chanin, and A. Hauchecorne (1991), Gravity waves in the middle atmosphere observed by Rayleigh lidar: 2. Climatology, *J. Geophys. Res.*, *96*(D3), 5169–5183.

Yoshiki, M., and K. Sato (2000), A statistical study of gravity waves in the polar regions based on operational radiosonde data, *J. Geophys. Res.*, *105*(D14), 17,995–18,011.

Yoshiki, M., N. Kizu, and K. Sato (2004), Energy enhancements of gravity waves in the Antarctic lower stratosphere associated with variations in the polar vortex and tropospheric disturbances, *J. Geophys. Res.*, *109*, D23104, doi:10.1029/2004JD004870.

Zhang, F., S. Wang, and R. Plougonven (2004), Uncertainties in using the hodograph method to retrieve gravity wave characteristics from individual soundings, *Geophys. Res. Lett.*, *31*, L11110, doi:10.1029/2004GL019841.

K. Sato, Department of Earth and Planetary Science, University of Tokyo, Tokyo 113-0033, Japan. (kaoru@eps.s.u-tokyo.ac.jp)

M. Yamamori, Department of Elementary Education, Tsuru University, 3-8-1 Tahara, Tsuru, Yamanashi 402-8555, Japan. (yamamori@tsuru.ac.jp)